eCG followed 72 hours later by 500 IU of im injection of hCG. Gilts were slaughtered 45 hours after hCG administration, and oocytes were recovered by flushing oviducts with Ca-free, Mg-free Dulbecco's phosphate-buffered saline (PBS) supplemented with 0.1% (w/v) bovine serum albumin (BSA). Oocytes were held in culture medium at 38.5°C in a water-saturated atmosphere of 5% CO_2 in air until required.
8. Electroactivation was typically 54 to 55 hours after hCG injection (3 to 4 hours after nucleus microinjection) in an activation medium containing 280 mM D-mannitol, 0.05 mM $CaCl_2$, 0.1 mM $MgSO_4$, and 0.01% (w/v) BSA. Pulses were delivered to cells in the chamber of an SSH-2 somatic hybridizer (Shimadzu, Kyoto, Japan). The number, intensity, and duration of pulses are detailed in Table 1. After the final pulse, oocytes were transferred for culture in medium supplemented with cytochalasin B (5 μg/ml) for 2 hours to prevent cytokinesis, after which culture was continued in fresh medium lacking cytochalasin B.
9. Embryo culture was in 100-μl droplets of medium under mineral oil at 38.5°C in a water-saturated atmosphere of 5% CO_2 in air. Unless stated otherwise, the culture medium was NCSU23 [R. M. Petters and K. D. Wells, *J. Reprod. Fertil.* **48** (suppl.), 61 (1993)] supplemented with 0.4% (w/v) BSA and 0.01% (w/v) cysteine. Two other media were used in preliminary studies: Beltsville embryo culture medium (BECM3) [J. R. Dobrinsky *et al.*, *Biol. Reprod.* **55**, 1069 (1996)] and modified Whitten's medium (mWM) [C. R. Youngs *et al.*, *J. Anim. Sci.* **71**, 1561 (1993)].
10. H. Funahashi *et al.*, *Theriogenology* **47**, 277 (1997).
11. A. E. Schnieke *et al.*, *Science* **278**, 2130 (1997).
12. J. B. Cibelli *et al.*, *Science* **280**, 1256 (1998).
13. K. J. McGreath *et al.*, *Nature* **405**, 1066 (2000).
14. Fibroblasts for nuclear transfer were obtained from fetuses produced by a Meishan × Meishan (black coat) cross 24 days after insemination. Fetuses were removed, and the tissue was cut into small pieces with fine scissors. Cells were dispersed by incubation for 3 hours at 4°C in PBS containing 0.25% (w/v) trypsin and 1 mM EDTA, after which they were washed once in Dulbecco's minimum essential medium (DMEM) supplemented with 10% (v/v) heat-inactivated fetal calf serum (FCS) (Gibco). Fetal cultures were established independently, without mixing, by plating at high density in DMEM supplemented with 10% (v/v) FCS. Culture was for two to six passages; with splits of 1:2 at each passage, we estimate that this represents 3 to 12 population doublings. Nucleus donor cell cultures were allowed to reach confluence and were cultured for a further 16 days without replenishment. Cultures were positive for proliferating cell nuclear antigen (PCNA) after 3 days but lost PCNA immunoreactivity after 10 days, suggesting that the cells were at G_0 after 16 days. PCR based on *ZFY*- and *SRY*-specific primers [E. Aasen and J. F. Medrano, *Biotechnology* **8**, 1279 (1990); D. Pomp *et al.*, *J. Anim. Sci.* **73**, 1408 (1995)] revealed the sex of fibroblast progenitors in each case. A normal karyotype for each cell culture was confirmed by Giemsa staining. Cultures derived from a single fetus were used in this study.
15. K. H. S. Campbell *et al.*, *Rev. Reprod.* **1**, 40 (1996).
16. A. Onishi *et al.*, data not shown.
17. T. Wakayama *et al.*, *Nature* **394**, 369 (1998).
18. Oocytes with a pronounced first polar body were orientated so that the position of the polar body was at 12, 3, or 6 o'clock. Removal of metaphase II chromosomes and the first polar body to generate enucleated oocytes for nuclear microinjection was by gentle aspiration with a beveled pipette of 25- to 30-μm external diameter, driven by a piezo-actuated unit (Prime Tech, Ibaraki, Japan). Piezo-actuation of the pipette permitted rapid penetration of the zona pellucida. Enucleation was in batches of 10 to 15 oocytes, at room temperature in NCSU23 medium containing cytochalasin B (5 μg/ml). Confirmation that the chromosomes had been completely removed was by staining with the DNA-specific dye Hoechst 33342 (Sigma) and examination under ultraviolet light. After successful enucleation, batches of oocytes were washed thoroughly in NCSU23 medium lacking cytochalasin B and returned to 38.5°C in a water-saturated atmosphere of 5% CO_2 in air until required.
19. Nucleus donor cells were resuspended from washed (three times in PBS) confluent cultures of nonreplenished fetal fibroblasts by gentle treatment with 0.25% (w/v) trypsin. The reaction was quenched by the addition of DMEM containing 10% (v/v) FCS, and the cells were pelleted. After a final wash in NCSU23, they were resuspended in 10 ml of NCSU23. A 10-μl aliquot was removed immediately before microinjection, mixed with 100 μl of NCSU23, and placed onto an inverted microscope stage. Batches of 10 to 15 enucleated oocytes were placed in the droplet for nuclear transfer. Each nucleus donor cell was approached by a flush-ended microinjection pipette (external diameter of 7 to 10 μm), and its plasma membrane was broken by gentle aspiration of the entire cell into and out of the pipette. The nucleus was gathered into the pipette and moved toward an enucleated oocyte. Piezo-actuation of the pipette again enabled rapid penetration of the zona pellucida and microinjection of the donor nucleus with minimal damage to the enucleated oocyte plasma membrane. Between manipulations, injection pipettes were washed in a droplet of NCSU23 containing 15% (w/v) polyvinylpyrrolidone (average relative molecular mass of 40,000). After donor nucleus microinjection, reconstituted preembryos were incubated at 38.5°C in a water-saturated atmosphere of 5% CO_2 in air for 3 to 4 hours before activation.
20. Z. Machaty *et al.*, *Biol. Reprod.* **59**, 451 (1998).
21. Preparation of surrogate mothers (surrogates) was as follows. Pregnant Landrace × Large White × Duroc crosses inseminated by Landrace boars were terminated at E21 to E40 by im injection of 0.2 mg of cloprostenol as described in (*7*), except that the second injection was accompanied by a reduction in eCG to 1000 IU. Induction of estrus in surrogates by im injection of hCG (500 IU) was 72 hours after the eCG injection. Six of the ten surrogates used in this study were artificially inseminated with Landrace boar semen 24 hours after hCG injection to generate "helper" embryos, and one side of the oviduct was flushed at the time of embryo transfer in preparation for the cloned embryos. The cloned embryos were transferred to oviducts 48 or 68 hours after hCG injection, 20 or 40 hours after electroactivation, respectively. One of the four noninseminated surrogates carrying embryos 40 hours after activation gave birth to the cloned offspring Xena.
22. J. R. Hill *et al.*, *Theriogenology* **51**, 1451 (1999).
23. D. N. Wells *et al.*, *Biol. Reprod.* **60**, 996 (1999).
24. T. Wakayama and R. Yanagimachi, *Nature Gen.* **22**, 127 (1999).
25. T. Wakayama, personal communication.
26. PCR analysis of genomic DNA in ear-punch biopsies of the surrogate mother, the cloned piglet Xena, and her fetal fibroblast progenitor culture was performed with 23 porcine-specific microsatellite markers [G. A. Rohrer *et al.*, *Genome Res.* **6**, 371 (1996)]. Samples were processed blind by means of a 373A Autosequencer supported by GenoTyper software (PE Biosystems, Foster City, CA). The following markers were used: SW286, SW840, SW957, SW133, SW274, SW373, SW491, SW741, SW839, SW742, SW1327, SW1311, SW122, SW435, SW540, SW942, SWR1021, SW1339, SW249, SWR426, SW524, SWR414, and SW717. Data from three marker sets (SW133, SW274, and SWR1021) were inconclusive. The characteristics of all remaining marker sets were shared between genomic DNA from the cloned piglet Xena and the fibroblast culture but were distinct from those of the Landrace surrogate mother.
27. M. J. Martin, *Biol. Reprod.* **63**, 109 (2000).
28. This work was supported in part by a Grant-in-Aid (Bio Cosmos Program) from the Ministry of Agriculture, Forestry and Fisheries of Japan. We are grateful to T. Wakayama and E. Nemeth for incisive comments and suggestions during manuscript preparation.

17 July 2000; accepted 27 July 2000

Twists in Catalysis: Alternating Conformations of *Escherichia coli* Thioredoxin Reductase

Brett W. Lennon,[1] Charles H. Williams Jr.,[2,3] Martha L. Ludwig[1,2]*

In thioredoxin reductase (TrxR) from *Escherichia coli*, cycles of reduction and reoxidation of the flavin adenine dinucleotide (FAD) cofactor depend on rate-limiting rearrangements of the FAD and NADPH (reduced form of nicotinamide adenine dinucleotide phosphate) domains. We describe the structure of the flavin-reducing conformation of *E. coli* TrxR at a resolution of 3.0 angstroms. The orientation of the two domains permits reduction of FAD by NADPH and oxidation of the enzyme dithiol by the protein substrate, thioredoxin. The alternate conformation, described by Kuriyan and co-workers, permits internal transfer of reducing equivalents from reduced FAD to the active-site disulfide. Comparison of these structures demonstrates that switching between the two conformations involves a "ball-and-socket" motion in which the pyridine nucleotide–binding domain rotates by 67 degrees.

TrxR from *E. coli* is a member of the pyridine nucleotide–disulfide oxidoreductase family of flavoenzymes. These enzymes use an active-site dithiol-disulfide to transfer reducing equivalents from FAD to external substrates (Fig. 1). The NADPH and FAD binding domains that constitute the TrxR monomer are related to corresponding domains in glutathione reductase, the prototype for this family of flavoenzymes (*1*). However, the organization of functional elements is different between *E. coli* TrxR and glutathione reductase. The active-site disulfide loop is in the NADPH domain in TrxR and in the FAD domain in glutathione reductase. Thus, the mechanisms

[1]Biophysics Research Division, [2]Department of Biological Chemistry, University of Michigan, Ann Arbor, MI 48109, USA. [3]Department of Veterans Affairs Medical Center, Ann Arbor, MI 48105, USA.

*To whom correspondence should be addressed. E-mail: mlludwig@umich.edu

of catalysis are also different in TrxR and glutathione reductase (*1*).

The structure of the flavin-oxidizing (FO) conformation of *E. coli* TrxR, a homodimer of 35-kD subunits, was determined by Kuriyan and colleagues (*2*). In this conformation (Fig. 2A), the disulfide loop of the enzyme adjoins the *re* face of the flavin in an orientation that allows reduction of the disulfide with concomitant oxidation of the flavin (reaction 2, Fig. 1). However, NADP(H) binds far from the flavin ring in this structure, and the active-site cysteines are buried where they cannot react with thioredoxin. Waksman *et al.* (*2*) modeled an alternative flavin-reducing (FR) conformation that would permit reduction of FAD by NADPH and dithiol-disulfide interchange with thioredoxin (reactions 1 and 3, Fig. 1).

We describe here the 3.0 Å structure of the FR conformation of TrxR from *E. coli*, obtained from a complex of thioredoxin and thioredoxin reductase (Figs. 2B and 3). We used thioredoxin as a "doorstop" to trap the FR state, cross-linking the two proteins with a disulfide connecting the active-site residues Cys^{138} of TrxR and Cys^{32} of thioredoxin (*3*). To establish the interactions of the FR form with pyridine nucleotides, we grew crystals in the presence of 3-aminopyridine adenine dinucleotide phosphate ($AADP^+$), an analog of nicotinamide adenine dinucleotide phosphate ($NADP^+$) (*4, 5*). The asymmetric unit of the *C*2 crystal form contains two dimers of the TrxR-$AADP^+$-Trx complex, related by a noncrystallographic twofold axis and connected by a bridge formed by extraneous $AADP^+$ (*5*). The structure was determined by molecular replacement and by refinement with the program CNS (*6*). Refinements that imposed strict equivalence of the four TrxR-Trx protomers reduced the residual indices, R and R_{free}, to 0.252 and 0.271, respectively; final values of R and R_{free} are 0.205 and 0.247 (Table 1). The domain interfaces and the interactions of TrxR with $AADP^+$ and Trx are well defined by the electron density, as illustrated in the composite omit maps (Fig. 4) (*7*).

Kinetic measurements (*8*) and the spectroscopic and redox properties of mutants and of cross-linked complexes with thioredoxin (*9–12*) have supported the conclusion that TrxR undergoes large conformational changes to allow the NADPH substrate and then the disulfide mediator to react with the flavin ring. The rate of interconversion of the two conformers has been deduced from kinetic studies of the reduction of wild-type and mutant TrxRs by NADPH (*8*). A slow phase of reduction, with an observed rate constant of 53 s^{-1} at 25°C, can be attributed to rearrangement of the FO structure to the alternate FR conformation that is able to react with NADPH. This step is likely to limit the rate of turnover (*8*).

Comparison of the FR and FO forms provides direct structural evidence for the conformational change that is required for catalysis (Fig. 2). In the conversion to the FR conformation, the NADPH domain rotates 67° about the axis shown in Fig. 2A, and moves toward the FAD domain by 1.4 Å (*13*). The pyridine ring of the $AADP^+$ that is bound to the FR form is stacked against the flavin ring in an orientation that would enable reduction of the flavin by the substrate, NADPH (*14*). The observed rotation is almost exactly as predicted by model building (*2, 15*).

The linkers between the NADPH and FAD domains act as a swivel. The rotation is achieved by rewrapping the antiparallel β strands ^{113}Gly-Ala-Ser-Ala-Arg-Tyr-Leu^{119} and ^{244}Gly-His-Ser-Pro-Asn^{248}, with key torsion angle changes at residues 113 to 116 and

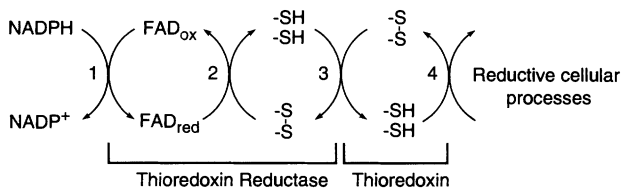

Fig. 1. Reaction catalyzed by thioredoxin reductase. Reducing equivalents from NADPH are transferred to the flavin cofactor, then to the enzyme disulfide (Cys^{135}-Cys^{138}), and finally to the disulfide (Cys^{32}-Cys^{35}) of the substrate, oxidized thioredoxin (*30*). Reduced thioredoxin is a reductant for ribonucleotide reductase and an activator of T7 DNA polymerase (*31, 32*).

Table 1. Summary of data collection and refinement statistics. Crystals were obtained as described (*4*). A crystal (0.08 mm by 0.08 mm by 0.26 mm), taken directly from the crystallization drop, was plunged into liquid nitrogen for data collection at −165°C on an R-AXIS IV image plate detector. Data were processed with the HKL package (*34*). The unit cell dimensions are a = 298.9 Å, b = 94.8 Å, c = 79.6 Å, β = 104.2° in space group *C*2, with two dimers per asymmetric unit. Cross-rotation searches with the program GLRF (*35*) used three search models: the dimer of FAD domains from TrxR (PDB code 1trb), a single NADPH domain from TrxR (PDB code 1trb), and thioredoxin (PDB code 2trx). Two clear orientations were obtained for the dimer of FAD domains, but the NADPH domains could not be found independently. Translation searches using CNS 0.9a (*6*) located both of the FAD dimers. All four NADPH domains were then found using the phased translation search implemented in CCP4 (*29, 36*), but further searches with the thioredoxin model failed to place the thioredoxins, which were located only after partial refinement. All refinements used CNS 0.9a (*6*), with the maximum likelihood target on amplitudes, and were interspersed with manual rebuilding using O (*37*). Rigid-body adjustment of the four TrxR chains, followed by simulated annealing (SA) in torsion space, allowed modeling of one of the four thioredoxins. Strict NCS constraints were then applied using a model of the single complete protomer (TrxR chain B and Trx chain B); torsional SA and positional refinement with all data to 2.95 Å reduced R to 0.340 and R_{free} to 0.366. Further torsional SA and positional refinement with strict NCS constraints relating the four protomers included bulk solvent corrections and adjustment of restrained B values, and reduced R to 0.252 and R_{free} to 0.271. After restrained NCS refinements, when R was less than 0.23, solvents were added to the model. In the final calculations, NCS restraints with a force constant of 150 kcal/mol were applied to the A-C and B-D pairs of protomers, and B factors were restrained within each chain and between NCS-related pairs of chains. At the conclusion of refinement, the model was verified by comparison with composite SA omit maps (*6*).

Data statistics	
Resolution range (Å) (last shell)	31 to 2.95 (3.06 to 2.95)
Total number of reflections (unique)	598,907 (45,732)
Completeness (%) (last shell)	99.8 (99.0)
R_{merge} (%)* (last shell)	8.4 (35.8)
$I/\sigma I$ (last shell)	15.0 (3.4)
Refinement statistics	
Reflections in working set (test set)	42,781 (2747)
R (%)†	20.5
R_{free} (%)‡	24.7
Number of nonhydrogen atoms	
Protein	12,980
Cofactors/nonprotein substrates	396
Solvents	236
RMSD from target values	
Bond lengths (Å)	0.0085
Bond angles (°)	1.44
Average isotropic B factors for all chains (Å^2)	
Backbone atoms (TrxR, Trx)	33.4, 80.4
Side-chain atoms (TrxR, Trx)	34.9, 80.5
FAD	21.6
$AADP^+$	32.9
Solvents	24.4*

*$R_{merge}(I) = \Sigma_{hkl}\Sigma_i|I_i(hkl) - \langle I_{hkl}\rangle| / \Sigma_{hkl}\Sigma_i|I_i(hkl)|$, where $\langle I_{hkl}\rangle$ is the average intensity for multiple observations of $I_{hkl,i}$ for symmetry-related reflections. †$R = \Sigma_{hkl}||F_{obs}| - |F_{calc}|| / \Sigma_{hkl}|F_{obs}|$ ‡R. factor calculated using the test set of 6% of the total reflections, which were not used in refinement.

residues 245 to 247 accounting for most of the displacement of the NADPH domain.

Analysis of the conformational change from FO to FR with the program DynDom (*16*) classifies it as a twisting of the domains relative to one another, rather than a domain closure or opening. The rearrangement can be described as a ball-and-socket rotation that exchanges smooth hydrophilic interfaces. The rotation axis (Fig. 2A) is approximately perpendicular to the interface between the NADPH and FAD domains, and it lies close to the linker strands that are positioned near one edge of the interface. In the conversion from the FO to the FR conformation, contacts between the NADPH domain and each of the two FAD domains of the dimer (Fig. 3) are broken and new contacts are formed (*17*). Many of the same residues from the NADPH domain contribute to both interfaces, but they contact different regions of the FAD domains (*7*). The interface between the NADPH and FAD domains decreases in area from ~1000 Å^2 in FO to ~630 Å^2 in FR, exposing the NADPH domain for interaction with thioredoxin.

As might be expected for a relatively facile rearrangement (*8*), no interdigitating side chains are found in the FO (*2*) or FR interfaces. Although most of the residues in the interface are hydrophilic, relatively few direct or solvent-bridged hydrogen bonds are formed between the FAD and NADPH domains (*17*). Most of the solvent molecules buried in the interfaces interact with residues from only one of the two surfaces. In the overall transition between FO and FR states, partners in the limited number of polar interactions are swapped, and side chains move to form the altered pairings. A preliminary study that examined structures generated by rotating the NADPH domain in 5° steps (*2*) found no barriers to the motion that could not be surmounted by adjustment of side chains.

Large motions of domains have been observed in a number of enzymes (*18, 19*). The motion in TrxR is different from other characterized conformational changes (*20*). Immunoglobulins undergo a ball-and-socket movement that involves bending at an elbow joint (*21*), whereas the motion in TrxR is purely a twisting of the ball within the socket. Iron binding to lactoferrin (*19*) induces a large rotation that involves breaking and remaking of interface contacts. However, in lactoferrin a domain rotates about an axis that is parallel to the interface, and the major contacts in the alternative conformations use different faces of the mobile domain. Swiveling of the phosphohistidine domain in pyruvate phosphate dikinase (*22*) may incorporate features of both the lactoferrin and TrxR motions.

The conformational change in TrxR exposes the disulfide loop and a substantial surface area for interaction with thioredoxin (Figs. 2 and 3) (*7*). Although the solvent-exposed regions of the Trx chains are not well defined, the regions constituting each of the TrxR-Trx interfaces are clearly visible in the electron density (Fig. 4). The disulfide cross-link (*3*) forms with little distortion of the local conformation of either partner. Thioredoxin packs against both the FAD and NADPH domains of TrxR, but it is the interactions with the NADPH domain that appear to be responsible for recognition of the protein substrate (*23*). A loop in thioredoxin (residues 70 to 75) occupies a complementary groove on the surface of the NADPH domain. Arg^{73} protrudes from the surface of thioredoxin (*24*) and interacts with Arg^{130} and nearby residues on one side of the groove in TrxR. Along the other side of the groove, Phe^{141} and Phe^{142} from TrxR fit into a hy-

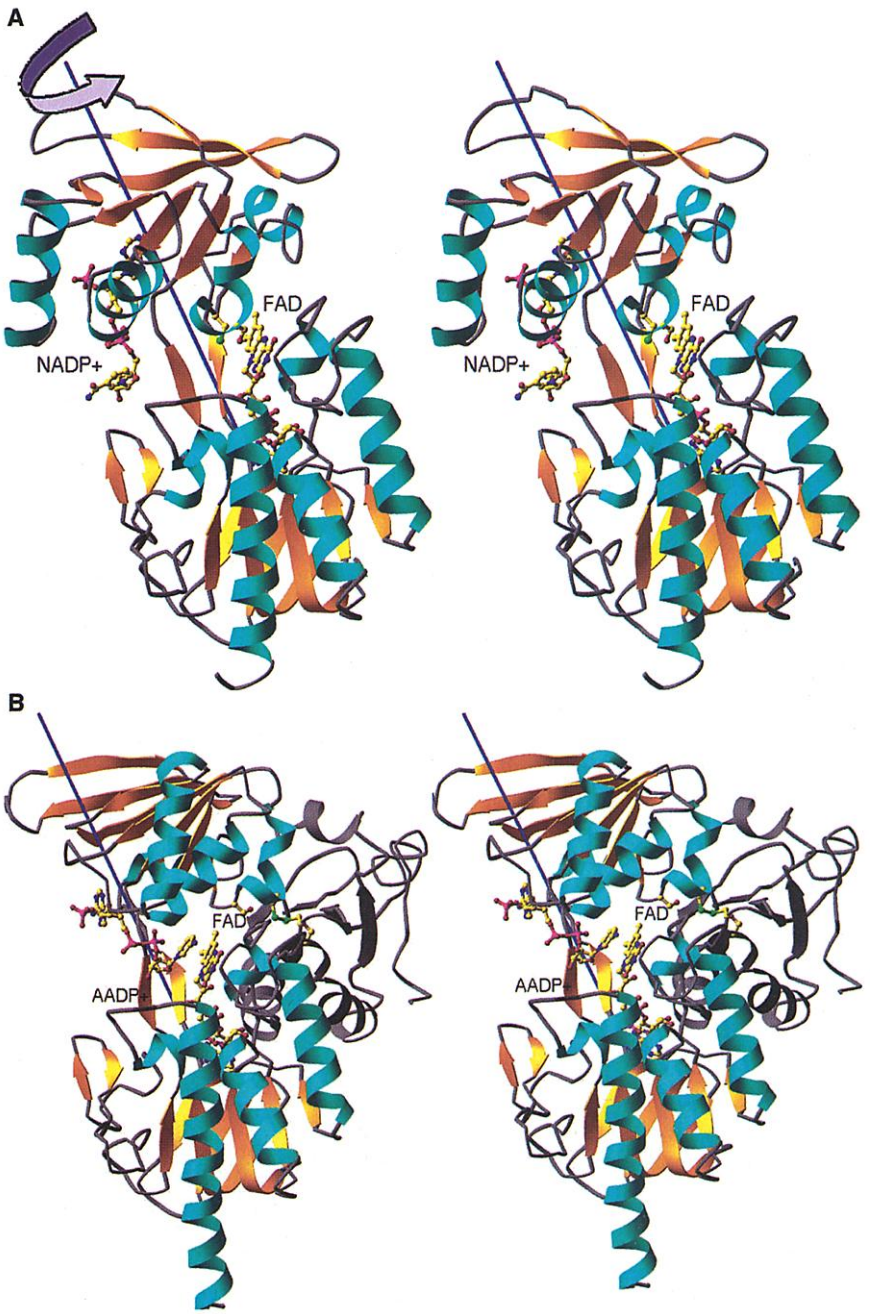

Fig. 2. Stereoviews showing the FO and FR states of thioredoxin reductase. In the conversion from FO (**A**) to FR (**B**), the upper NADPH domain (comprising residues 120 to 243) rotates 67° about the axis shown in blue. This very large rotation is evident from comparisons of the positions of the bound pyridine nucleotides and major helices. In (A), which was drawn using coordinates of the Cys^{138} → Ser mutant of TrxR complexed with NADP$^+$ (PDB code 1tdf), the FO conformation (*2*) permits reaction of reduced FAD with the active-site disulfide. In (B), the FR conformation permits reaction of pyridine nucleotides with the FAD and reaction of thioredoxin with the active-site cysteine (Cys^{138}) of TrxR. Thioredoxin (gray) is cross-linked to TrxR in the FR structure. [Figures 2 to 4 were prepared with the program Ribbons (*33*).]

drophobic pocket on thioredoxin formed by Trp^{31}, Ile^{60}, Gly^{74}, and Ile^{75} (Fig. 4) (*7*). Another hydrophobic patch near Ile^{75} of thioredoxin, proposed to be important in interactions of thioredoxin with other proteins (*25*), is exposed to solvent and does not contact TrxR.

Domain rotation is used by TrxR to solve the steric problem that arises when reactions between prosthetic groups and enzyme-bound mediators are part of the catalytic cycle. An alternative strategy has evolved in the related glutathione reductase (GR), the best known of the pyridine nucleotide–disulfide flavoenzymes. In GR, bound FAD receives reducing equivalents from NADPH at one face of the isoalloxazine ring and reduces a disulfide loop positioned at the opposite face (*26*). The small substrate can directly access the active-site dithiol that adjoins the flavin ring. Thus, there is no need for major conformational changes in glutathione reductase. The high molecular weight (monomer = 55 kD) thioredoxin reductases in humans and *Plasmodium falciparum* are homologous to GR, with the active-site disulfide in the FAD domain, but react with large substrates. To communicate between the disulfide that is reduced by FAD and thioredoxin substrates, these enzymes use a second redox mediator (a selenosulfide or disulfide, respectively) (*12, 27, 28*) that is not present in *E. coli* TrxR. Hence, the *E. coli* and mammalian TrxR enzymes have evolved different mechanisms for the transfer of reducing equivalents from the FAD prosthetic group to a large substrate.

The structure of the FR form of *E. coli* TrxR shows that TrxR rearranges using an unusual domain motion: a ball-and-socket rotation in which large areas of the interdomain surfaces glide by one another. This rearrangement, which allows a buried cofactor to communicate with a large substrate, is essential for catalysis.

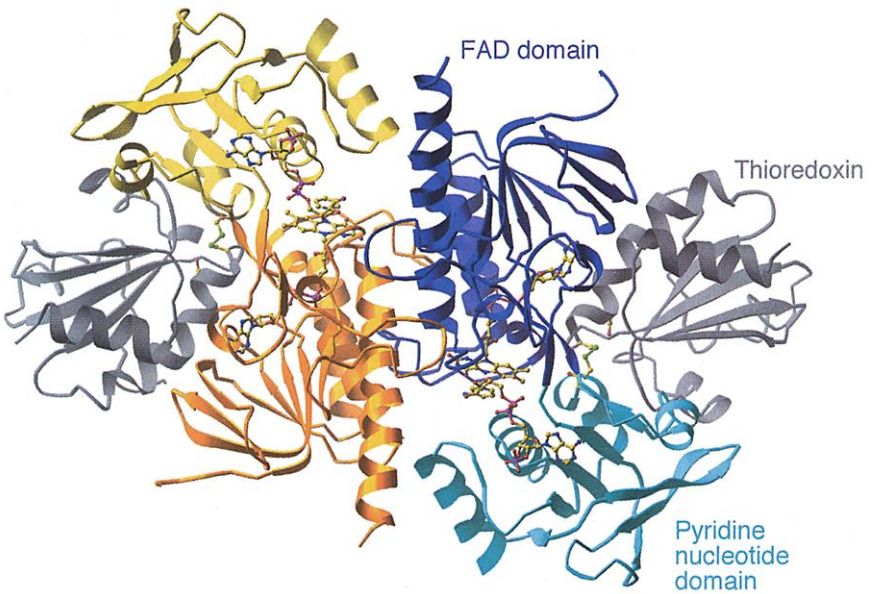

Fig. 3. The dimer of the TrxR-Trx complex with TrxR in the FR conformation, viewed down the molecular dyad. Blue and cyan denote one monomer of the TrxR dimer; gold and yellow denote the second monomer. The TrxR-Trx protomer on the right is designated A; the protomer on the left is B. These are related to protomers C and D, respectively, by NCS. Each NADPH domain contacts both of the FAD domains of the dimer. The thioredoxin substrates (gray), which bind and react at opposite ends of the TrxR dimer, are accommodated by the FR conformation. FAD, $AADP^+$, and the TrxR-thioredoxin cross-link (sulfurs in green) are drawn in ball-and-stick mode. [See (*7*) for more detailed views of the active site and the domain interfaces.]

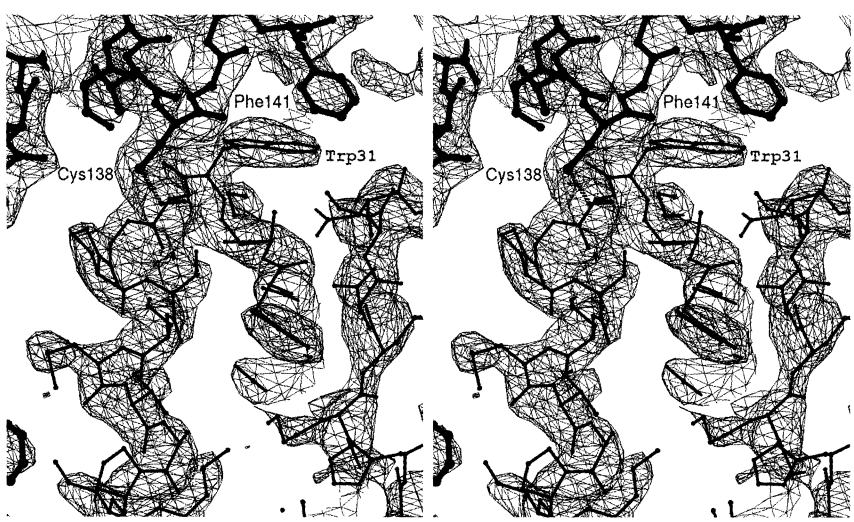

Fig. 4. A stereoview of the refined model and the electron density in the vicinity of the disulfide cross-link connecting TrxR and Trx in protomer A. The density is from a composite omit map (*6*) at 3 Å resolution. This view, showing the region corresponding to the helix of Trx that follows the cross-link at Cys^{32} (dashed), displays part of the hydrophobic pocket formed by residues from both Trx and TrxR (see text). Contours are drawn at 1σ.

References and Notes

1. C. H. Williams Jr., in *Chemistry and Biochemistry of Flavoenzymes*, F. Müller, Ed. (CRC Press, Boca Raton, FL, 1992), vol. 3, chap. 5.
2. G. Waksman, T. S. R. Krishna, R. M. Sweet, C. H. Williams Jr., J. Kuriyan, *J. Mol. Biol.* **236**, 800 (1994).
3. The complex with a disulfide linking Cys^{32} of thioredoxin to Cys^{138} of TrxR was prepared as described (*9*). Cys^{35} of thioredoxin and Cys^{135} of TrxR were mutated to serines. The thiol reagent 5,5′-dithiobis(2-nitrobenzoic acid) was used to form an intermediate mixed disulfide between the active-site cysteine Cys^{32} of Trx and thionitrobenzoic acid. The mixed disulfide was isolated and reacted with the $Cys^{135} \rightarrow$ Ser mutant of TrxR. The cross-linked protein is stable because the mutant serines are unable to attack the intermolecular disulfide. The Cys^{32}-Cys^{138} disulfide is probably the physiologically relevant one (*12*).
4. Crystals were grown at 22°C in hanging drops by mixing 2 μl of the TrxR-Trx complex (*3*) at 20 mg/ml in 10 mM Hepes (pH 7.0) with 1 μl of ~80 mM $AADP^+$ and 2 μl of a well solution prepared by mixing 0.1 M cacodylate (pH 6.0) with 50% saturated $(NH_4)_2SO_4$ and 24% (w/v) polyethylene glycol (PEG, molecular weight 3350), then centrifuging for 5 min at 1000*g*. The supernatant, enriched in PEG 3350, was diluted to 72 to 74% with water.
5. There is a region of positive density (peak >8σ) in the $(|F_{obs}| - |F_{calc}|)$ map, centered on the noncrystallographic symmetry (NCS) twofold axis relating the two dimers in the asymmetric unit. The shape suggests that excess $AADP^+$ forms a bridge between the dimer molecules, adopting two orientations to satisfy the local symmetry. We were unable to build satisfactory models of $AADP^+$ into this density. The bridging density touches residues from the FAD domains of the B and D protomers of the TrxR-Trx complexes. Because the A and C protomers do not contact the bridge but are essentially identical to the B and D protomers, it seems unlikely that the dimer contact at the NCS axis has influenced the arrangement of domains (*18*) within the protomers.
6. A. T. Brünger *et al.*, *Acta Crystallogr.* **D54**, 905 (1998).
7. For supplementary figures, see *Science* Online (www.sciencemag.org/feature/data/1051414.shl).
8. B. W. Lennon and C. H. Williams Jr., *Biochemistry* **36**, 9464 (1997).
9. P.-F. Wang, D. M. Veine, S. H. Ahn, C. H. Williams Jr., *Biochemistry* **35**, 4812 (1996).
10. S. B. Mulrooney and C. H. Williams Jr., *Protein Sci.* **6**, 2188 (1997).

11. D. M. Veine, K. Ohnishi, C. H. Williams Jr., *Protein Sci.* **7**, 369 (1998).
12. D. M. Veine, S. B. Mulrooney, P.-F. Wang, C. H. Williams Jr., *Protein Sci.* **7**, 1441 (1998).
13. See the animation at *Science* Online (www.sciencemag.org/feature/data/1051414.shl).
14. The C4 atom of $AADP^+$ and the N5 atom of FAD are separated by 3.4 Å (*7*).
15. The structure of glutathione reductase was used by Kuriyan and co-workers (*2*) to predict the domain packing in the FR structure of TrxR. They aligned the FAD domains of glutathione reductase and TrxR and then matched the NADPH domain of TrxR to the corresponding domain of glutathione reductase. The rotation applied to the NADPH domain to build the model (66°) is almost identical to the observed rotation, but the core main-chain atoms of the modeled NADPH domain are displaced from those observed in our structure by a root mean square deviation of 4.9 Å.
16. S. Hayward and H. J. C. Berendsen, *Proteins* **30**, 144 (1998).
17. Hydrogen bonds and ion pairs were assigned by the program CONTACTS (*29*). In both the FO and FR structures, two protein-protein hydrogen bonds connect the FAD and NADPH domains of the same monomer chain. In the FO structure, eight hydrogen bonds link the NADPH domain of one monomer to the FAD domain of its partner chain; only three such interactions are found in the FR structure. There are similar numbers of well-ordered waters in the domain interfaces (17 for the FO, 21 for the FR conformation).
18. G. E. Schulz, *Curr. Opin. Struct. Biol.* **1**, 883 (1991).
19. M. Gerstein *et al.*, *J. Mol. Biol.* **234**, 357 (1993).
20. M. Gerstein and W. Krebs, *Nucleic Acids Res.* **26**, 4280 (1998).
21. M. Lesk and C. Chothia, *Nature* **335**, 188 (1988).
22. O. Herzberg *et al.*, *Proc. Natl. Acad. Sci. U.S.A.* **93**, 2652 (1996).
23. The average temperature factor, $\langle B \rangle$, for the thioredoxin chains, ~80 $Å^2$, is much larger than $\langle B \rangle$ for the rest of the cross-linked complex (Table 1), but the residues at the interfaces with TrxR are more ordered ($\langle B \rangle$ = 63 $Å^2$).
24. H. Eklund, F. K. Gleason, A. Holmgren, *Proteins* **11**, 13 (1991).
25. H. Eklund *et al.*, *EMBO J.* **3**, 1443 (1984).
26. E. F. Pai and G. E. Schulz, *J. Biol. Chem.* **258**, 1752 (1983).
27. L. D. Arscott, S. Gromer, R. H. Schirmer, K. Becker, C. H. Williams Jr., *Proc. Natl. Acad. Sci. U.S.A.* **94**, 3621 (1997).
28. T.-W. Gilberger, B. Bergmann, R. D. Walter, S. Müller, *FEBS Lett.* **425**, 407 (1998).
29. Collaborative Computational Project No. 4, *Acta Crystallogr.* **D50**, 760 (1994).
30. C. H. Williams Jr., *FASEB J.* **9**, 1267 (1995).
31. L. Thelander and P. Reichard, *Annu. Rev. Biochem.* **48**, 133 (1979).
32. D. F. Mark and C. C. Richardson, *Proc. Natl. Acad. Sci. U.S.A.* **73**, 780 (1976).
33. M. Carson, *Methods Enzymol.* **277**, 493 (1997).
34. Z. Otwinowski and W. Minor, *Methods Enzymol.* **276**, 307 (1997).
35. L. Tong and M. G. Rossmann, *Methods Enzymol.* **276**, 594 (1997).
36. H. M. Doesburg and P. T. Beurskens, *Acta Crystallogr.* **A39**, 368 (1983).
37. T. A. Jones, J. Y. Zou, S. W. Cowan, M. Kjeldgaard, *Acta Crystallogr.* **A47**, 110 (1991).
38. We thank D. M. Veine for purification of the $Cys^{35} \rightarrow$ Ser mutant of thioredoxin. Supported by NIH fellowship award GM18723 (B.W.L.) and by NIH grants GM16429 (M.L.L.) and GM21444 (C.H.W.). Coordinates for this structure have been deposited in the Protein Data Bank (accession code 1F6M).

17 April 2000; accepted 30 June 2000

Asef, a Link Between the Tumor Suppressor APC and G-Protein Signaling

Yoshihiro Kawasaki,[1] Takao Senda,[2] Takao Ishidate,[1] Ryo Koyama,[1] Tsuyoshi Morishita,[1] Yoriko Iwayama,[2] Osamu Higuchi,[1] Tetsu Akiyama[1,3]*

The *adenomatous polyposis coli* gene (*APC*) is mutated in familial adenomatous polyposis and in sporadic colorectal tumors. Here the APC gene product is shown to bind through its armadillo repeat domain to a Rac-specific guanine nucleotide exchange factor (GEF), termed Asef. Endogenous APC colocalized with Asef in mouse colon epithelial cells and neuronal cells. Furthermore, APC enhanced the GEF activity of Asef and stimulated Asef-mediated cell flattening, membrane ruffling, and lamellipodia formation in MDCK cells. These results suggest that the APC-Asef complex may regulate the actin cytoskeletal network, cell morphology and migration, and neuronal function.

Mutations of the tumor suppressor gene *APC* are responsible for familial adenomatous polyposis, a dominantly inherited disease characterized by multiple adenomatous polyps in the colon (*1*). The *APC* gene is also somatically mutated in most sporadic colorectal tumors. Consistent with its role as a tumor suppressor, overexpression of *APC* blocks cell cycle progression from the G_1 to S phase (*2*). The product of the *APC* gene interacts with various proteins, including β-catenin, a key component of the Wnt/Wingless signaling transduction pathway that plays important roles in a number of developmental processes and in tumorigenesis (*3*). APC is thought to be involved in the degradation of β-catenin through its interaction with β-catenin, GSK-3β, and Axin or the closely related factor conductin/Axil (*4*). APC also interacts with EB1 and the human homolog of the *Drosophila* Discs large (hDLG) through its COOH-terminal region (*5*, *6*). Furthermore, APC possesses an armadillo repeat domain, which is thought to be involved in protein-protein interactions. To obtain new insights into the function of APC, we attempted to identify proteins that interact with the armadillo repeat domain of APC.

We screened a human fetal brain library using the armadillo repeat domain of APC as target, and isolated a gene that we have named *Asef* (for APC-stimulated guanine nucleotide exchange factor) (*7*). The human full-length *Asef* cDNA encodes a protein of 619 amino acids with motifs found in the Dbl family of proteins (Fig. 1, A and B) (*8*). Asef contains the Dbl homology (DH), Pleckstrin (PH), and Src homology 3 (SH3) domains. Northern blot analysis of Asef revealed a mRNA of 3.6 kb that is highly expressed in mouse brain (*9*).

To confirm that APC and Asef interact directly, we created a fusion protein (APC-arm) consisting of the armadillo repeat domain of APC and glutathione-*S*-transferase (GST). We examined the ability of this fusion to interact with the fragment of Asef (Asef-M in Fig. 2A) (*10*). The in vitro–translated APC-arm interacted with GST–Asef-M, but not with GST alone (Fig. 2B). Likewise, in vitro–translated Asef-M interacted with GST–APC-arm, but not with the armadillo repeat domain of β-catenin fused to GST (GST–β-catenin–arm) or GST alone.

To identify the region of Asef responsible for its interaction with APC, we performed two-hybrid assays using deletion fragments of Asef. Mutants lacking amino acids 73 to 126 were negative for interaction with APC, whereas a fragment containing amino acids 73 to 126 was positive (Fig. 2A). This indicates that the APC-binding region may reside in the NH_2-terminal region upstream of the SH3 domain.

We next examined whether endogenous Asef associates with APC in vivo. A lysate from embryonic rat brain was subjected to immunoprecipitation with antibodies to Asef (anti-Asef) followed by immunoblotting with anti-APC (*11*). Asef was identified as an 85-kD protein and coimmunoprecipitated with APC (Fig. 2C). Similarly, immunoprecipitation of the lysate with anti-APC followed by immunoblotting with anti-Asef revealed an association between APC and Asef. Coprecipitation of Asef and APC was inhibited by preincubation of the antibodies with

[1]Laboratory of Molecular and Genetic Information, Institute for Molecular and Cellular Biosciences, University of Tokyo, 1-1-1 Yayoi, Bunkyo-ku, Tokyo 113, Japan. [2]Department of Anatomy I, Nagoya University School of Medicine, 65 Tsurumai-cho, Showa-ku, Nagoya, Aichi 466, Japan. [3]Department of Oncogene Research, Institute for Microbial Diseases, Osaka University, 3-1 Yamadaoka, Suita, Osaka 565, Japan.

*To whom correspondence should be addressed. E-mail: akiyama@imcbns.iam.u-tokyo.ac.jp